Genomic evidence reveals three sequential W-autosome fusions in *Heliconius* butterflies

Nicol Rueda - M[1,7], Carolina Pardo-Diaz[1], Gabriela Montejo-Kovacevich[2], W. Owen McMillan[3], Krzysztof M. Kozak[3,4], Carlos F. Arias[3,5], Jonathan Ready[5,6], Shane McCarthy[7], Richard Durbin[2,7], Chris D. Jiggins[2], Joana I. Meier[2,7*], Camilo Salazar[1*+]

*These authors contributed equally to this work.

[1]Biology Program, Faculty of Natural Sciences, Universidad del Rosario, Bogotá, Colombia. 111221

[2]Department of Zoology, University of Cambridge, Cambridge, CB2 3EJ, United Kingdom

[3]Smithsonian Tropical Research Institute, Panama

[4]Museum of Vertebrate Zoology, UC Berkeley, USA

[5]Data Science Lab, Office of the Chief Information Officer, Smithsonian Institution, Washington, DC, United States

[5]Institute for Biological Sciences, Federal University of Pará - UFPA, R. Augusto Corrêa, 1 - Guamá, Belém - PA, 66075-110, Brazil

[6]Centre for Advanced Studies of Biodiversity - CEABIO, Guamá Science Park, Lot 11, Avenida Perimetral da Ciência km 01 - Guamá, Belém - PA, 66075-750, Brazil

[7]Tree of Life Programme, Wellcome Sanger Institute, United Kingdom

[+]camilo.salazar@urosario.edu.co (CS)

Abstract

Sex chromosomes are evolutionarily labile in many animals and sometimes fuse with autosomes, creating so-called neo-sex chromosomes. Fusions between sex chromosomes and autosomes have been proposed to reduce sexual conflict and to promote adaptation and reproductive isolation among species. Recently, advances in genomics have fuelled the discovery of such fusions across the tree of life. Here, we discovered multiple fusions leading to neo-sex chromosomes in the *sara/sapho* clade of the classical adaptive radiation of *Heliconius* butterflies. *Heliconius* butterflies generally have 21 chromosomes with very high synteny. However, the five species in the *sapho* subclade show large variation in chromosome number ranging from 21 to 60. We found that the W chromosome is fused with chromosome 4 in all of them. Two sister species pairs showed subsequent fusions between the W and chromosomes 9 or 14, respectively. These sequential fusions between autosomes and sex chromosomes make *Heliconius* butterflies an ideal system for studying the role of neo-sex chromosomes in adaptive radiations and the degeneration of sex chromosomes over time. Our findings emphasize the capability of WGS technology to detect neo-sex chromosomes even when sex chromosomes are not explicitly assembled.

Author Summary

Fusions between sex chromosomes and autosomes are thought to have the potential to resolve sexual conflict and enhance local adaptation or reproductive isolation between species. Here, we discovered such fusions in *Heliconius* butterflies. *Heliconius* butterflies mostly have a very stable karyotype with 21 chromosomes and high synteny across species. However, the five species in the *sapho* subclade have up to 60 chromosomes, suggesting that they have undergone many chromosomal fissions. We document that in addition to the fissions, the *sapho* subclade also showed multiple fusions between the female-specific sex chromosome (W) and autosomes. We found a W-4 fusion shared by all five species and additional W fusions with chromosomes 9 and 14 shared by two species each. Even though in many *sapho* subclade species the autosomes have undergone fissions, the chromosomes fused with the W represent the full-length autosomes, as seen in other *Heliconius* species, suggesting that fusing to the W protected them from fissions. Our study reveals the power of short-read sequencing to discover neo-sex chromosomes and showcases *Heliconius* butterflies as a promising system for studying the causes and consequences of sex chromosome evolution.

41 # Introduction

42 Sex chromosome-autosome (Sex-A) fusions contribute to the evolution of neo-sex
43 chromosomes (1,2), but it remains unclear what promotes them. Sexually antagonistic
44 selection, direct selection, genetic drift, meiotic drive, and sheltering of deleterious
45 mutations have all been suggested as possible drivers of Sex-A fusions (3–6). Sexually
46 antagonistic selection is thought to favour the fusion of sex chromosomes with
47 autosomes harbouring genes under sexually antagonistic selection (7). There is limited
48 evidence for this hypothesis e.g. in sticklebacks (8), *Drosophila* flies (9), warblers (10)
49 and butterflies (11). Sex-A fusions can also become fixed due to meiotic drive (including
50 holocentric drive in holocentric organisms) (12), such as female meiotic drive elements
51 on W/X-A fusions that preferentially end up in the egg instead of the polar bodies (13).
52 An alternative hypothesis is deleterious mutation sheltering, which Sex-A fusions are
53 favoured because they prevent the expression of recessive deleterious alleles in the
54 heterogametic sex (3). As with other chromosomal rearrangements, Sex-A fusions can
55 reduce recombination and potentially strengthen reproductive isolation (14,15). For
56 instance, in the Japanese threespine stickleback *Gasterosteus aculeatus,* a Sex-A
57 fusion resulted in a neo-X chromosome that linked loci underlying behavioural isolation
58 traits and hybrid sterility (4). Sex-A fusions may also facilitate adaptation, such as the
59 Sex-A fusion in *Cydia pomonella* (Tortricidae), which apparently linked two insecticide-
60 resistance genes and genes involved in detoxifying plant metabolites (16).

61 Cytogenetic and genomic studies revealed that Sex-A fusions have occurred many
62 times across vertebrates (6,17,18) and invertebrates such as spiders (19,20), *Drosophila*
63 flies (21,22) or true bugs of the genus *Dysdercus* (23). In Lepidoptera (butterflies and
64 moths), examples of Sex-A fusions include *Danaus* (24,25) and *Leptidea* butterflies
65 (26,27), among others (16,28–31). Compared to taxa with a single centromere per
66 chromosome, the holocentric chromosomes of Lepidoptera may facilitate fusions, as they
67 are less likely to cause segregation problems during cytokinesis and thus reduce hybrid
68 fitness (32). Nonetheless, butterflies and moths have remarkably constrained
69 chromosome evolution (33), with most species having a ZW or Z0 sex determination
70 system and a haploid chromosome number ranging between 28 and 32, except for few
71 groups that have experienced extensive fission and fusion events (31,34).

72 Here, we focused on *Heliconius* butterflies, which have undergone 10 ancestral
73 fusions and thus display 20 autosomes, along with Z and W sex chromosomes with high
74 collinearity across species (35). Only a few species in the genus differ in this ancestral
75 chromosome number, especially species in the *sara/sapho* clade, with some having up to
76 60 chromosomes (36). The *sara/sapho* clade comprises 12 species (31) that are different
77 from other *Heliconius* due to their inability to synthesize cyanogens (compounds that deter
78 predators) thus forcing them to rely on sequestered plant toxins (37). A subclade of seven
79 species within the *sara/sapho* clade shows particularly high diversification rates (38) and
80 high number of chromosomes (36).

81 We assembled a reference genome of *Heliconius sara*, a species that shows the normal
82 karyotype of 21 chromosomes. We found that it was fully collinear with the other two
83 species with chromosome-level assemblies. Next, we generated whole-genome
84 resequencing data from 114 individuals of all seven species of the *sara/sapho* clade with
85 high diversification rates to completely resolve their phylogenomic relationships and
86 study genomic differences between the species. We discovered that the *sapho*
87 subclade, which shows the high number of chromosomes in some species, exhibits
88 fusions between the W chromosome and autosomes (W-A fusions). One W-A fusion is
89 shared by all five species, whereas two additional W-A fusions are shared by two
90 species each. The autosomes fused to the W represent the full-length chromosomes,
91 indicating that they have not undergone the same high rates of fissions as the unfused
92 autosomes. These sequential W-A fusions make the *Heliconius sapho* subclade a prime
93 study system for the evolution of neo-sex chromosomes.

94 Results

95 High-quality reference genome assembly for *Heliconius sara*

96 We assembled the genome of *Heliconius sara* using two laboratory-reared females from
97 a stock population originating from Panama (S1 Table). Using the first individual
98 (BioSample SAMEA8947140), we obtained 24 Gbp PacBio CLR data with a coverage of
99 50x and an N50 subread length of 16.5 kb 122 Gbp of 10X linked-read Illumina data with
100 a coverage of 294x. From the second individual (BioSample SAMEA8947139), we

101 obtained 137 Gbp Hi-C Illumina data with 111x coverage. The final assembled genome
102 consists of 348.8 Mbp in 384 scaffolds. The contig N50 was 8.2 Mbp and that of scaffold
103 N50 was 17.8 Mbp. Our genome showed the highest contiguity (S2 Table) and BUSCO
104 statistics (S3 Table) of some currently published *Heliconius* genomes. The BUSCO
105 completeness, using the Lepidoptera gene set, achieved 98.2% single-copy BUSCOs
106 and less duplicated, fragmented, and missing BUSCOs than in the genomes of *H. erato*
107 (39), *H. melpomene* (40) and *H. charithonia* (41) (S3 Table). We assigned the largest
108 twenty-two scaffolds to 20 autosomes and one scaffold to the Z chromosome based on
109 synteny with the *Heliconius melpomene* genome. *H. sara* chromosomes are collinear
110 with this genome, as well as with *H. erato* and *H. charithonia* (S1 Fig). For more
111 information on the genome see
112 https://tolqc.cog.sanger.ac.uk/durbin/jiggins/Heliconius_sara/ and
113 https://www.ncbi.nlm.nih.gov/datasets/genome/GCA_917862395.2/.

114 The W chromosome did not assemble well, as is commonly seen in lepidopteran
115 genomes (31). We thus used whole genome resequencing data from 114 individuals
116 collected during this study (see below "Whole-genome resequencing dataset section") to
117 assign scaffolds to the W chromosome based on sequencing depth differences between
118 males and females. Among the 360 scaffolds not assigned to a specific chromosome,
119 32 exhibited a higher mean depth in females than in males in *Heliconius sara*. This
120 pattern suggests that these 32 scaffolds likely constitute a part of the W chromosome
121 (S2 Fig). Interestingly, the reads from the *sapho* subclade species (*H. antiochus*, *H.*
122 *sapho*, *H. hewitsoni*, *H. eleuchia*, and *H. congener*) did not align to these 32 scaffolds,

suggesting that W chromosome of these species is either too divergent from the *H. sara* W chromosome (S2 Fig) or not present. The W scaffolds in *H. sara* correspond to a single homolog in *H. charithonia* (S1C Fig).

Whole-genome resequencing dataset

A total of 114 individuals were successfully whole-genome resequenced. Our dataset exhibits high taxonomic completeness covering all 7 species within the *sara/sapho* subclade (*H. sara*, *H. leucadia*, *H. antiochus*, *H. sapho*, *H. hewitsoni*, *H. eleuchia*, and *H. congener*) and 19 out of the 28 described subspecies (42) (S1 Table). The average mapping percentage to the *H. sara* genome was 95.56% (range: 77.38% - 99.14%) (S1 Table). We observed a strong phylogenetic signal in the mapping proportion and, consequently, in the proportion of missing data per individual (S1 Table and S3 Fig). The average coverage was 97.7%, 97.6%, and 96.4% for *H. sara* specimens, its sister species *H. leucadia*, and the *sapho* group, respectively. One *H. congener* and one *H. antiochus* individual exhibited a particularly high proportion of missing data (19.5% and 39.5%, respectively) and low mean coverage (7.4X and 9.1X, respectively) (S1 Table and S3 Fig), and were thus excluded from further analyses.

Phylogenetic analysis reveals two main subclades and uncovered incongruence across the genome

We reconstructed a Maximum Likelihood (ML) phylogenetic tree using 183,282,470 concatenated sites. This phylogeny separated individuals into two main subclades, consistent with the PCA analyses (S4 Fig): (i) *sara* and (ii) *sapho* (Fig 1). The *sara* subclade is composed of two species, namely *H. sara* and *H. leucadia*, where *H. sara* is subdivided into an Andean subgroup (*H. s. magdalena, H. s. sprucei,* and *H. s. elektra*) and an Amazonian subgroup (*H. s. sara*). The *sapho* subclade was split into two well-resolved lineages (*H. antiochus* and a subclade composed of two monophyletic groups: *H. eleuchia/H. congener* and *H. sapho/H. hewitsoni*). *H. antiochus* appeared as a monophyletic group split into an Andean group (*H. a. aranea* and *H. a. araneides*), and an Amazonian group (*H. a. antiochus* and *H. a. salvini*) (Fig 1). *H. antiochus* nested into the *sapho* subclade, whereas *H. hewitsoni* was found to be sister to *H. sapho,* thus resolving the previously undetermined position of these species (38).

To complement the concatenated phylogeny, we also reconstructed a species tree with Astral. The species phylogeny closely mirrored the genome wide phylogeny (S5A Fig). Although *H. hewitsoni* and *H. sapho* were recovered as sister species, their branch lengths (measured in coalescence units) (S5A Fig) were short. This was also the case for the subspecies of *H. eleuchia,* where *H. e. eleusinus* and *H. e. primularis* sometimes group with *H. congener* (S5A Fig). These phylogenetic discordances were also evident in the DensiTree analysis visualising 271 phylogenies together (S5 Fig).

We found a strong phylogenetic incongruence across chromosomes. The whole-genome topology was only recovered on eight chromosomes (S6-S27 Fig), while nine chromosomes showed *H. congener* appearing as sister either to *H. e. eleuchia* or to a clade composed of *H. e. eleusinus* + *H. e. primularis* (S6-S27 Fig). Similarly, the position of *H. hewitsoni* relative to *H. sapho* varied on eight chromosomes (S6–S27 Fig). Interestingly, we observed sex-specific clustering on three chromosomes (S27B Fig). On chromosome 4 (Chr4), all species in the *sapho* subclade showed females and males forming separate clades within each species, whereas the males of *H. congener* and *H. eleuchia* formed a shared clade and their females formed a shared clade (S27B and S9 Fig). Sex-specific clades were also observed on chromosome 9 in *H. sapho* and *H. hewitsoni* (S27B and S14 Fig) and on chromosome 14 in *H. eleuchia* and *H. congener* (S27B and S19 Fig).

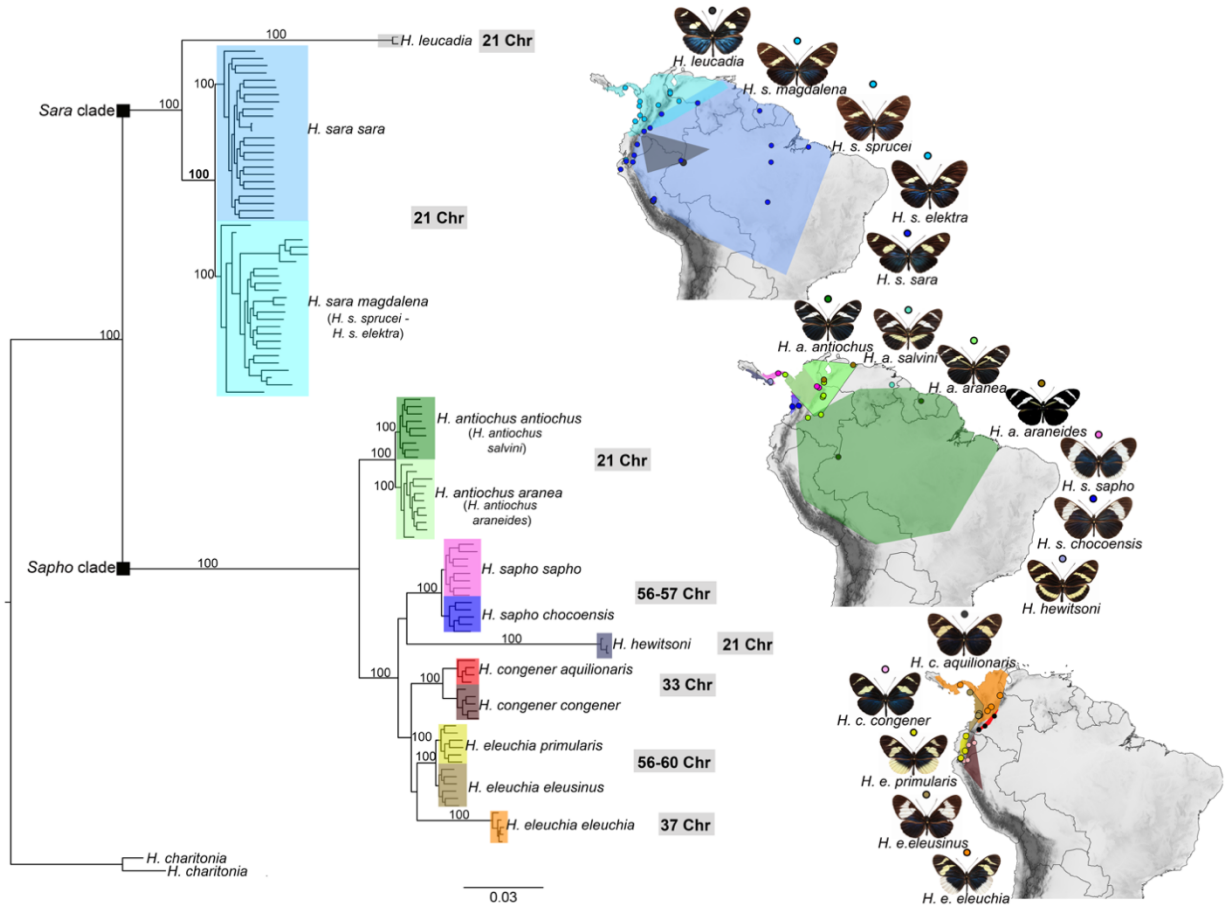

Fig 1. Phylogeny and distribution of the *sara/sapho* clade. Genome-wide ML phylogeny, highlighting the position of the *Sara* and the *Sapho* subclades, with bootstrap support values on the branches. The distribution of all 17 subspecies in the clade from (43) is shown, where dots represent sampling locations in the present study. Each of the 17 subspecies is represented by a single colour, that is the same in the phylogeny and the distribution. The chromosome number of each species is shown in grey rectangles (43). The species' distribution map was created using the free and open source QGIS (44), with a base shapefile obtained from https://www.naturalearthdata.com/downloads/10m-cultural-vectors/ and an elevation raster from https://srtm.csi.cgiar.org/srtmdata/.

Haplotype-based phylogenetic analysis on chromosomes 4, 9 and 14

The grouping by sex we observed in the phylogenetic trees of Chr4, Chr9 and Chr14 suggest possible fusions between these autosomes and either the Z or W chromosome, or possibly both (females of *Heliconius* are ZW and males are ZZ) (42). As females of Lepidoptera lack crossing over and their meiosis is achiasmatic, they do not recombine (45). This means that if the W chromosome is involved in the fusion (Fig 2A), the Sex-A fusion would be restricted to females and the fused chromosome would tend to accumulate mutations and/or structural variants leading to divergence from its unfused homologous. The unfused chr4 would become a neo-Z2 chromosome in all species of the *sapho* subclade, chr9 would become a neo-Z3 in *H. sapho,* and *H. hewitsoni* and chr14 would become a neo-Z3 in *H. congener* and *H. eleuchia*. Alternatively, if the Z chromosome is involved in the fusion (Fig 2B), females would initially still have the unfused homologue (neo-W) that would start to accumulate mutations and/or structural variants, leading to the divergence from the Z-fused homologue. If the sex-autosome fusion was with the Z in the *sapho* subclade, chr4 would become neo-W2 in all five species, chr9 would become neo-W3 in *H. sapho* and *H. hewitsoni* and chr14 would become neo-W3 in *H. congener* and *H. eleuchia*. Lastly, it is possible that both the Z and the W fused to the autosomes, leading to neo-W and neo-Z, reducing the number of chromosomes.

Under either fusion to the Z or the W, we predict i) site-specific genealogies where each female has one haplotype that forms part of the same clade as the male haplotypes, while the other haplotype forms a female-specific clade (hereafter called female-specific haplotype clustering), ii) low genetic differentiation (F_{ST}) on Chr4, Chr9, and Chr14, due to higher divergence between males and females within populations and lower variation between populations if they share the same sex-autosome fusions (see “Patterns of genetic differentiation”), iii) high proportion of sites where all females are heterozygous due to the presence of two different haplotypes (see “Sex-specific differences in heterozygosity and mean depth”), and iv) low sequencing depth in females due to poor mapping of the female-specific haplotypes that have accumulated mutations and structural variants (see “Sex-specific differences in heterozygosity and mean depth”) (Fig 2).

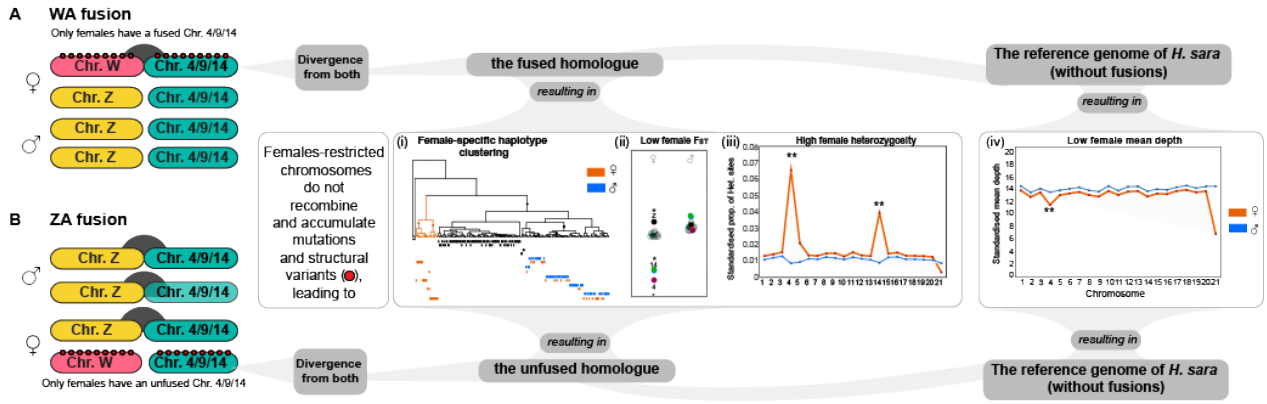

Fig 2. Scenarios of Sex-A fusions involving either the W or Z chromosomes. Scenario of (A) WA fusion and (B) ZA fusion for Chr4, Chr9 and Chr14 differentiating the expected pattern by sex: (i) Female-specific haplotype clustering, (ii) low female Fst, (iii) high female heterozygosity and (iv) low female mean depth. For more details see main text. Yellow: Z chromosome. Pink: W chromosome. Green: autosome. Dark-grey semicircles: fusions. Red dots: mutations and/or structural variants. Lastly, it is possible that both the W and Z chromosomes may have fused with these autosomes, resulting in a neo-W and neo-Z sex chromosome constitution.

226 Consistent with our hypotheses, we identified 218,839 SNPs on Chr4, where all males
227 within the *sapho* subclade were homozygous, and most females were heterozygous (<1
228 female per species was homozygous). To study the phylogenetic relationships among
229 male and female haplotypes at these sites, we phased our dataset and inferred marginal
230 phylogenies from ancestral recombination graphs constructed using Relate. We
231 subsampled the dataset to every 1000th SNP with high female heterozygosity (214
232 SNPs). At 31% of these sites, we recovered the expected phylogeny with a female-specific
233 haplotype clade (Fig 3A). The sites displaying this pattern were distributed across the
234 entire chromosome and were not concentrated in a specific region (Fig 3B). Another set
235 of SNPs (53%) exhibited genealogies where female haplotypes from at least two species
236 within the *sapho* subclade clustered as expected for a Sex-A fusion (S28 Fig). The
237 remaining sites (16%) exhibited a mixed signal, similar to the unphased phylogenetic tree
238 obtained for the entire chromosome (S27B Fig). This is likely due to phasing errors where
239 the fused and unfused homologues of the females are mixed. On Chr9, we found 66,344
240 sites where *H. sapho* and *H. hewitsoni* exhibited the expected pattern, given a Sex-A
241 fusion. In this case, we found that the 23% of the 66 sampled sites displayed the expected
242 genealogy (S29A Fig). The remaining 77% of the SNPs showed a mixed signal as in Chr4
243 (Fig S27B). Finally, on Chr14 for *H. eleuchia* and *H. congener*, we identified 57,953 sites
244 with the described pattern. Among the 57 subsampled sites, 44% showed the expected
245 genealogical clustering (S30A Fig), while the remaining 56% displayed the mixed signal
246 described before for Chr4 and Chr9 (Fig S27B).

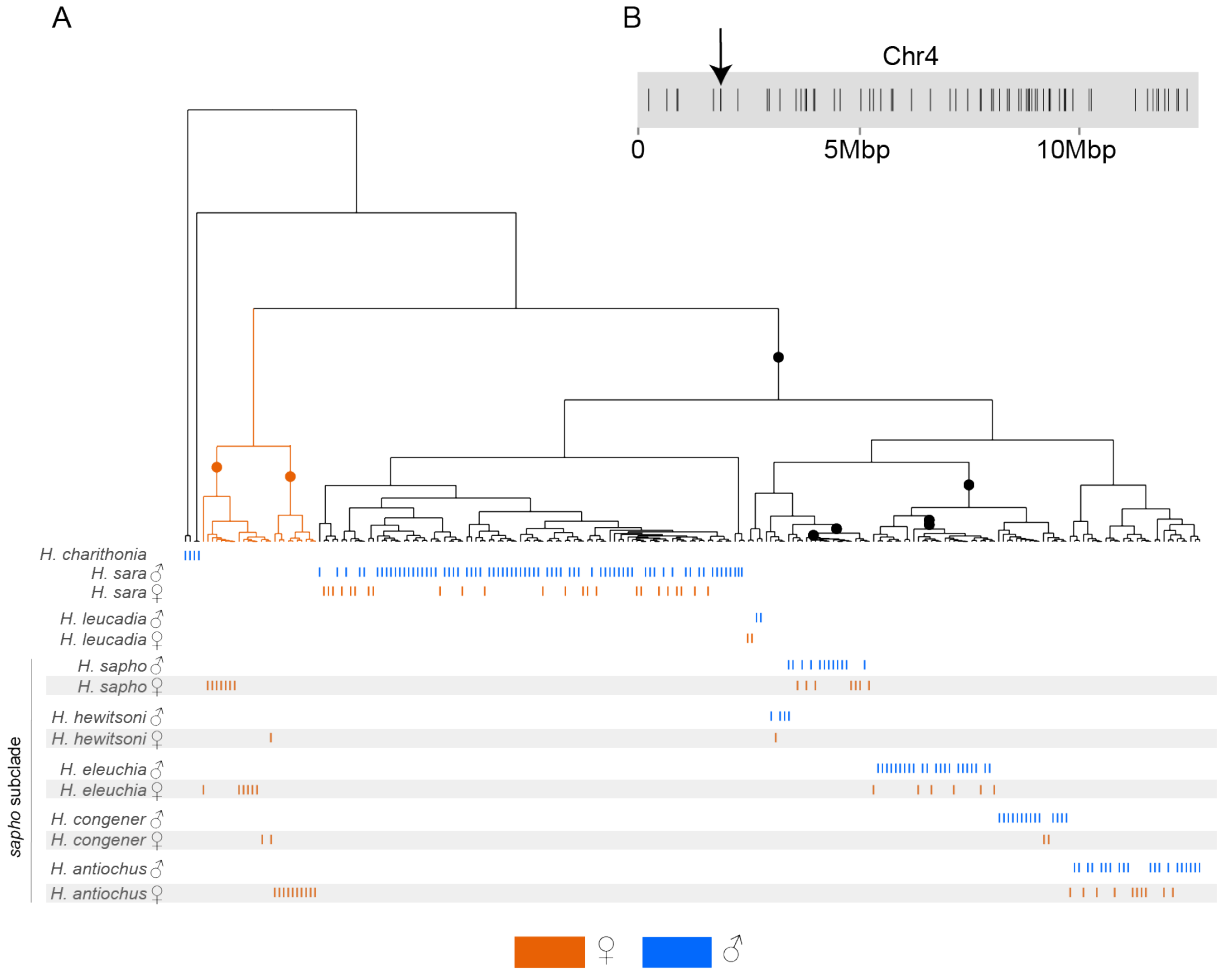

Fig 3. Marginal tree for one of the SNPs on Chr4. Genealogy of the SNP 1,900,983 in Chr4 showing a pattern fully consistent with a Sex-A fusion; a total of 66 subsampled SNPs across this chromosome showed the same pattern. Each vertical line represents an individual haplotype, and the haplotypes of all individuals are shown differentiating those of females (orange) from those of males (blue). Note that one allele of the females in the *sapho* subclade clustered with the alleles of males, while the other female allele formed a separate group (highlighted in orange). (B) Position of each of the 66 SNPs in Chr4 that showed genealogies consistent with a Sex-A fusion; they were not clustered in a specific region but rather distributed along the entire chromosome. The position of the SNP 1,900,983, whose genealogy shown in A, is indicated by an arrow.

Patterns of genetic differentiation

Genomic differentiation (F_{ST}) was strongest between *H. sapho* vs. *H. hewitsoni* followed by *H. congener* vs. *H. eleuchia,* and Andean vs. Amazonian *H. antiochus* (average F_{ST} = 0.33, 0.26, and 0.07 respectively) (S31 Fig). *H. sara* vs. *H. leucadia* were the least differentiated pair (average F_{ST} = 0.05) (S31 Fig). We also observed elevated F_{ST} values on the Z chromosome compared to autosomes in all but one comparison (*H. eleuchia* vs. *H. congener*) (S31 Fig). In line with predictions from sex-autosome fusions in the *sapho* subclade, Chr4 showed lower than average F_{ST} values in the *sapho* subclade, but not in *H. sara* vs. *H. leucadia* (Fig 4A and S31 Fig). This pattern is expected if the females have a haplotype that is more similar to the females of the other population or species compared than to their second haplotype or the males of their own population, thus leading to high within-population diversity and low between-population differences. Chr9 showed lower F_{ST} in *H. sapho* vs. *H. hewitsoni* Chr9 (Fig 4A and S31 Fig), and Chr14 in *H. eleuchia* and *H. congener* (Fig 4A and S31 Fig). The same pattern was observed when we compared F_{ST} between subspecies (S32 – S34 Fig). In line with expectations (Fig. 2), the observed pattern of lower F_{ST} on Chr4, Chr9, and Chr14 was exclusive to females and absent in males across all comparisons mentioned above within the *sapho* subclade (Fig 4B). The observed differences in F_{ST} between males and females were statistically significant for these three chromosomes (Wilcoxon test $p < 0.01$) (S35 Fig). The F_{ST} values of these chromosomes within females were also significantly lower compared to those of the other chromosomes (Wilcoxon test $p < 0.01$) (S35 Fig).

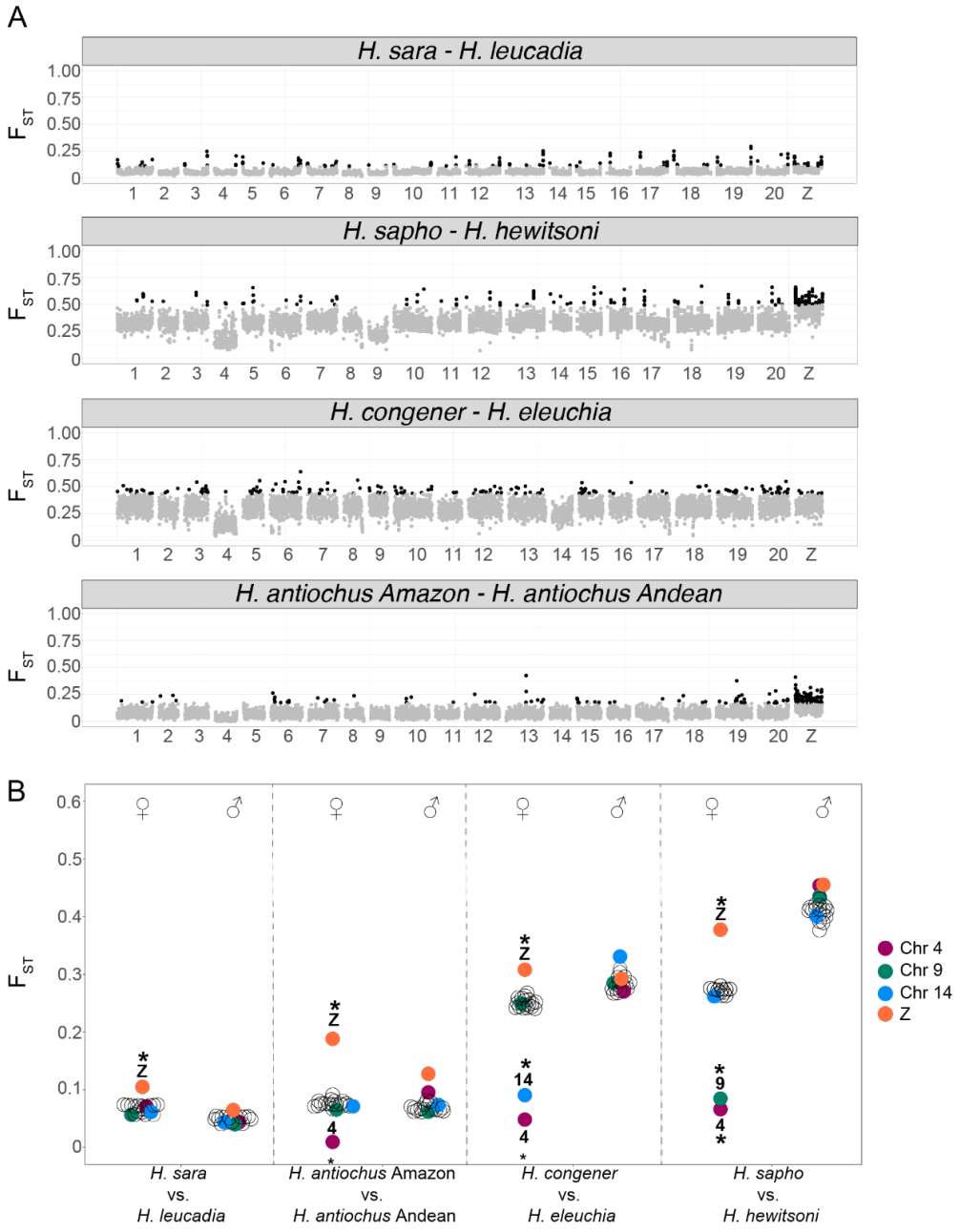

Fig 4. Genome-wide divergence (F_{ST}) in the *sara/sapho* clade. (A) F_{ST} between pairs of species. Each point represents a 50Kb window, whereby the. the top 5% windows are shown in black. The numbers below correspond to *H. sara* chromosomes. Subspecies comparisons are shown in S32-S34 Figs. (B) F_{ST} between pairs of species by sex. Each circle represents a chromosome, and chromosomes with evidence of Sex-A fusions are colour coded (* indicates outlier chromosomes, $p<0.01$). The observed reduction in F_{ST} in females is due to higher genetic diversity within species due to the divergence between the sex chromosome-fused and unfused haplotypes in females.

287 ## Sex-specific differences in heterozygosity and mean depth

288 Consistent with our hypotheses (Fig 2), Chr4, Chr9, and Chr14 showed striking sex-
289 specific differences in the proportion of heterozygous sites and mean depth only in the
290 species of the *sapho* subclade, supporting three sequential fusions of these chromosomes
291 with the Z or W chromosomes or both (Fig 5). The strongest difference in the proportion
292 of heterozygous sites was observed on Chr4, where females of *H. eleuchia*, *H. congener*,
293 *H. sapho*, *H. hewitsoni,* and *H. antiochus* showed a higher proportion of heterozygous
294 sites than males and the other autosomal chromosomes in females (Fig 5B). Females of
295 *H. eleuchia* and *H. congener* also showed a high proportion of heterozygous sites on
296 Chr14 and in *H. hewitsoni* and *H. sapho* on Chr9 (Fig 5B). Differences between males
297 and females were significant on these three chromosomes for all species of the *sapho*
298 subclade (Wilcoxon test, $p < 0.01$) (S36 Fig), except for *H. hewitsoni* where differences
299 could not be tested due to low sample size. The proportion of heterozygous sites of
300 females was also significantly higher for Chr4 than for the other chromosomes in *H.*
301 *eleuchia*, *H. sapho*, *H. antiochus* and *H. congener* (Wilcoxon test, $p < 0.01$) (S36 Fig). The
302 same was true for Chr14 in *H. eleuchia* and *H. congener,* and Chr9 in *H. sapho* (Wilcoxon
303 test, $p < 0.01$) (S36 Fig). A high proportion of heterozygous sites was not observed in the
304 females of the species *H. sara* and *H. leucadia* on any chromosome (Fig 5 and S36 Fig).
305 Chromosome Z exhibited lower proportion of heterozygous sites than autosomal
306 chromosomes in females across all species (Fig 5 and S36 Fig).

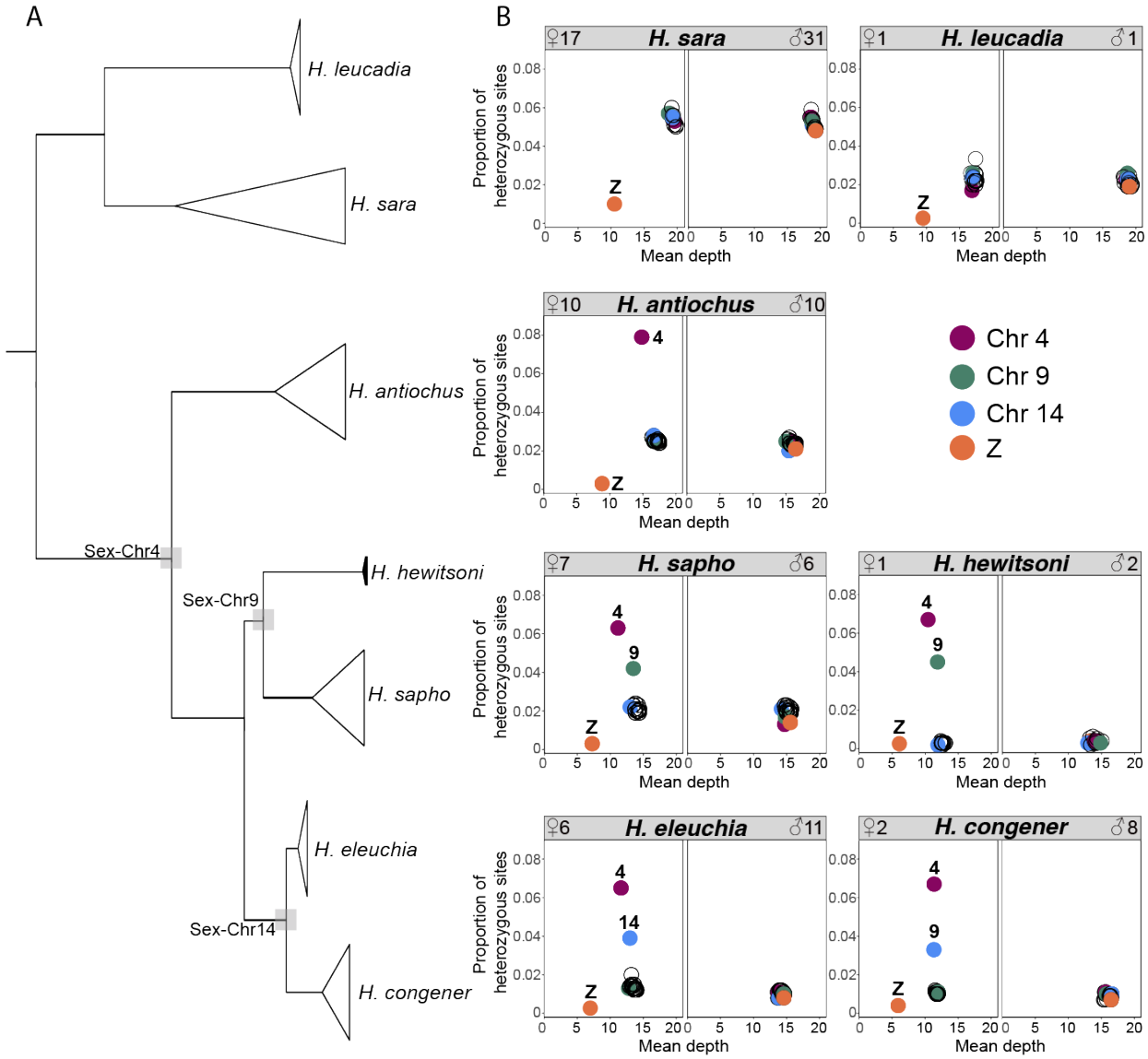

Fig 5. Genome-wide topology and patterns of heterozygosity and sequencing depth across the genome. (A) Genome-wide topology with grey squares highlighting nodes with putative Sex-A fusions. (B) The proportion of heterozygous sites vs. mean sequencing depth per chromosome, by sex and in each species. Each circle represents a chromosome, and chromosomes with evidence of Sex-A fusions are colour coded. The high heterozygosity in females is due to the presence of the fusion in only one of the haplotypes, which becomes divergent from its counterpart. The low mean depth is because the haplotype limited to females diverged enough to be difficult to map onto the reference genome of *H. sara.*

315 Females of *H. eleuchia*, *H. sapho*, *H. hewitsoni,* and *H. antiochus* also showed a reduced
316 mean depth on chromosome 4, whereas the mean depth on that chromosome in males
317 was normal (Fig 5B). However, these differences were only significant in *H. sapho*
318 (Wilcoxon test, $p \leq 0.01$) (S37D Fig). This pattern was not true for Chr14 in *H. eleuchia*
319 and *H. congener*, nor Chr9 for *H. sapho* and *H. hewitsoni* (Figs 5). The mean depth of
320 Chr4 was also lower than that of all other autosomes in females of *H. sapho* (Wilcoxon
321 test, $p \leq 0.01$) (S37D Fig). However, this was not true for Chr14 and Chr9 (S37 Fig).

322 The sliding window analyses on Chr4, Chr9, and Chr14 revealed that the excess
323 heterozygosity in females is present in most windows along the entire chromosomes
324 (i.e., it is not concentrated in a specific region on the chromosomes; Wilcoxon test, p
325 <0.01) (Fig 6 and S38-S40 Fig). Also, mean depth values were lower for females than
326 males in most windows on Chr4 for *H. eleuchia, H. congener, H. sapho* and *H.*
327 *antiochus*, Chr9 for *H. sapho* and Chr14 for *H. eleuchia* and *H. congener* (Wilcoxon test,
328 p <0.01) (Fig 6 and S38-S40 Fig). As expected, some peaks of high sequencing depth,
329 likely due to expansions of repeats or duplications were also visible in both females and
330 males (Fig 6). Interestingly, one female of *H. congener* has a region of eight windows on
331 Chr4 with very high sequencing depth (Fig 6), indicating that repeat expansions may still
332 be ongoing. There were also few windows on Chr4, Chr9, and Chr14 where females
333 exhibited both lower mean sequencing depth than males and (almost) no heterozygous
334 sites (highlighted with a grey rectangle) (Fig 6). In these regions, the female-specific
335 haplotype likely diverged too much from the reference genome to map well and thus the
336 heterozygosity is low in females because only one haplotype is represented in the data.

H. sara and *H. leucadia* were the only species in the clade that did not show sex-specific patterns in heterozygosity and mean depth in Chr4, Chr9 and Chr14 (Fig 6 and S38-S40 Fig). Interestingly, the heterozygosity in females of *H. congener* and *H. sapho* dropped at the end of Chr14 and Chr9, respectively, to values similar to those of the males (S38 Fig), indicating that the last part of these chromosomes may not be fused to a sex chromosome in this species. However, the mean depth pattern did not change in these regions (S38 Fig).

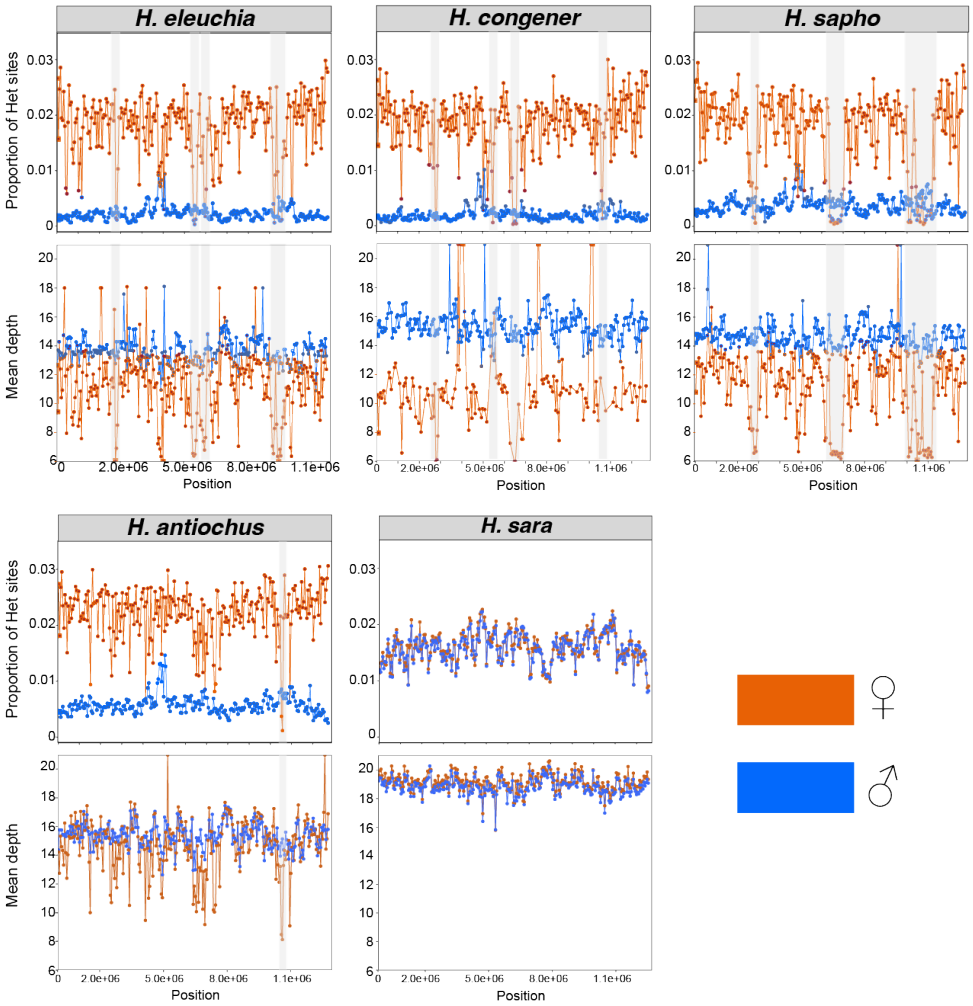

345 **Fig 6. Patterns of heterozygosity and depth across Chr4. Proportion of heterozygous (Het) sites and mean**
346 **sequencing depth in 50 kb sliding windows for each** species. Males are shown in blue and females in orange. Grey
347 rectangles highlight regions where females show very low sequencing depth and no heterozygous sites, suggesting
348 that the female-limited haplotype diverged enough to become unmappable to the *H. sara* reference genome. The
349 mean depth figures were trimmed to a maximum value of 20 in order to better visualize the differences between
350 sexes.

351 Evidence for three W-autosome fusions

352 In order to elucidate if the W or Z chromosome or both are involved in the sex-autosome
353 fusions, we produced Illumina Hi-C data for a female *H. congener* (0.71 Gbp) and a
354 male *H. sapho* (0.73 Gbp). We mapped the Hi-C data of these two *sapho* subclade
355 individuals and the *H. sara* Hi-C data produced for the reference genome to our *H. sara*
356 genome and to a previously published *H. charithonia* genome which has the W
357 assembled (41). In line with phylogenetic distances, the proportion of reads mapping to
358 the *H. sara* reference genome were much higher (96%, 93% and 92%) than to the *H.*
359 *charithonia* reference genome (69%, 70%, 71% for *H. sara*, *H. congener* and *H. sapho*,
360 respectively. The mean mapping quality for all three species against both genomes
361 exceeded a Phred quality score of 35.

362 We did not observe an excess of Hi-C contacts either between autosomes or
363 between autosomes and sex chromosomes in the *H. sara* female (Fig 7A), as expected
364 if the sex-autosome fusions were only in the *sapho* subclade. The Hi-C signal of the *H.*
365 *sapho* male and the *H.* congener female showed that their genomes are split into 56 and
366 33 chromosomes, respectively (Fig 7B-C), consistent with findings by Brown et al (36)

367 and suggesting a high number of chromosome fissions. However, no fusion was
368 observed in the *H. sapho* male, suggesting that the Chr4 and Chr9 fusions are likely not
369 with the Z, but with the W (Fig 7B). In contrast, the female *H. congener* showed an
370 excess of contacts between Chr4 and Chr14, in line with a fusion (Fig 7C). There was
371 no excess of Hi-C contacts between Chr4 and Chr14 with the Z chromosome (Fig 7C
372 and 7D), indicating that the Chr4 and Chr14 are likely fused with the W instead. Even
373 though there is signal of Hi-C contact between these chromosomes and the W, the low
374 mapping rates of Illumina reads of the *sapho* subclade to the W of the *Heliconius sara*
375 genome (S2 Fig) likely explains the absence of a stronger signal.

376 As the Hi-C signal of chromosome fusions in the *H. congener* female represents
377 a mix of signals from the fused and unfused haplotypes (Fig 7C-D), we phased the Hi-C
378 data across the chromosomes of interest (Chr4, Chr14, W, Z) and used *chomper* (46) to
379 split the Hi-C data into two subsets of read pairs representing the two haplotypes (47.5%
380 and 52.2% of the read pairs in each subset). The excess of Hi-C contacts between Chr4
381 and Chr14 was completely absent on one haplotype (Fig 7E) and very strong on the
382 other haplotype (Fig 7F). The Hi-C contacts between Chr4 and Chr14 are unevenly
383 distributed (Fig 7E), suggesting not only a fusion between these chromosomes but also
384 the presence of other chromosomal rearrangements such as inversions or
385 translocations.

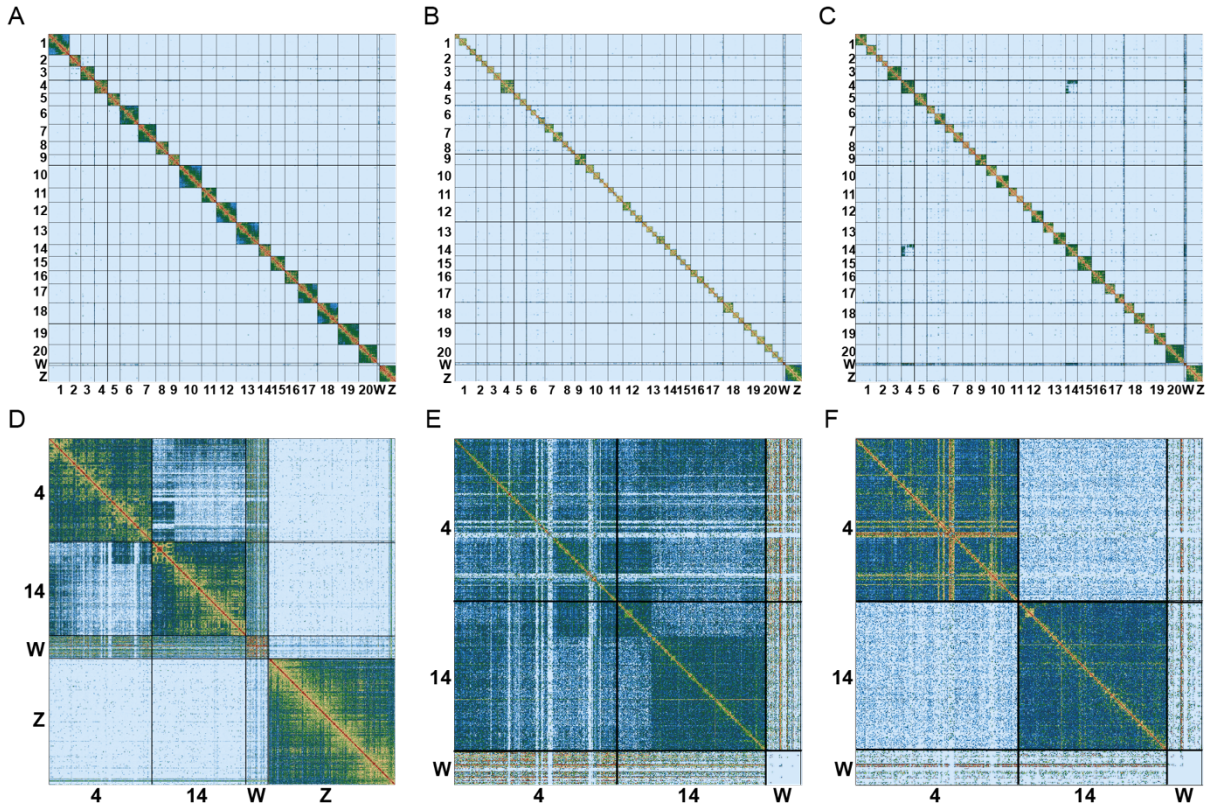

Fig. 7. Hi-C contact density map confirmed a high number of chromosome fissions and W-A fusions in the *sapho* subclade. Hi-C contact heatmaps of the *H. sara* reference genome of (A) the *H. sara* female, (B) the *H. sapho* male, and (C) the *H. congener* female. Note that the chromosomes of the *H. sara* reference genome are labelled and their boundaries are denoted with vertical and horizontal black lines. (D) Zoom in (C) showing Hi-C contacts on Chr4, Chr14, ChrW, and ChrZ. (E) Hi-C reads assigned to one of the two haplotypes in the *H. congener* female showing the W-A fusion. (F) Hi-C reads assigned to the other haplotype in the *H. congener* female showing no evidence of a fusion.

Discussion

We found evidence of three W-A fusions involving Chr4, Chr9, and Chr14 in the evolution of the *sara/sapho* clade in *Heliconius* butterflies. These autosomes seem to have fused with the W chromosome as supported by: (i) females with one haplotype each forming part of female-specific haplotype clade, (ii) low F_{ST} values in females, (iii)

398 high heterozygosity and low mean depth in females, and (iv) excess of Hi-C contacts in
399 the *H. congener* female but not in the *H. sapho* male. Because females are the
400 heterogametic sex in butterflies and show no recombination (45), the W-A fusion is
401 restricted to females and generates female-specific haplotypes that do not recombine
402 with the unfused chromosomes. This results in genealogies where one haplotype of the
403 females clusters with male haplotypes while the other haplotype of the females, the
404 fused one, forms a separate female-specific clade. Each female shows many
405 heterozygous sites on the ancestral Chr4 and depending on the species also on Chr9 or
406 Chr14, as it has inherited from the mother a fused W-4(-9/14) that never recombines
407 and accumulates mutations and structural variants and from the father unfused Z
408 chromosomes (Z1=ancestral Z, Z2=ancestral Chr4 (and Z3=ancestral Chr9 or Chr14).
409 This, in turn, increases variation within species and reduces variation between them, as
410 females share the fused haplotypes with females of other species, thus leading to
411 reduced $F_{ST.}$ Chr4 showed female-specific haplotype clustering and high female
412 heterozygosity throughout the chromosome in all five species of the *sapho* subclade,
413 indicating that the W chromosome fused with Chr4 in the ancestor of this group. In line
414 with an old fusion and increasing degeneration, females showed a high proportion of
415 heterozygous sites in most of the chromosome, and in some regions, the fused
416 haplotype had degenerated so much that mapping to the *H. sara* genome failed, leading
417 to low sequencing depth and the absence of heterozygous sites. Similar, but less strong
418 patterns of female-biased heterozygosity are found in Chr9 in *H. sapho* and *H.*
419 *hewitsoni*, and in Chr14 in *H. eleuchia* and *H. congener.* In line with younger fusions and

420 weak degeneration, the sequencing depth of females matches that of the males on
421 those chromosomes, indicating that the female-specific haplotypes still map well to the
422 *H. sara* genome.

423 Sex-A fusions in Lepidoptera usually involve the Z chromosome (31,47), but this
424 does not seem to be the case in *Heliconius*. Our *H. sapho* male (ZZ) did not have any
425 chromosome fusions, indicating that neither Chr4 nor Chr9 in that species is fused to the
426 Z, whereas Hi-C data from the female *H. congener* supports a fusion on one of the
427 haplotypes between Chr4 andChr14 with the W chromosome. Thus, in this species, the
428 unfused Chr4 and Chr14 become neo-Z2 and neo-Z3 chromosomes, respectively, and
429 the fused chromosome becomes the neo-W chromosome. Although the absence of a
430 fusion with the Z in the female *H. congener* clearly points to a W fusion, Hi-C contacts
431 between Chr4-Chr14 and the W are weak. This is likely due to the divergence of the W
432 in the *sapho* subclade from that of *H. sara*, making it difficult to map reads against this
433 reference (S2 Fig). Alternatively, the original W in the *sapho* subclade may have an
434 independent origin to that in *H. sara* or it may have been lost completely, as suggested
435 for other Lepidoptera (47).

436 The finding of multiple W-A fusions in the *sapho* subclade is particularly striking,
437 since this group is known for its high number of chromosomes compared to all other
438 *Heliconius* species that was also confirmed with our Hi-C data. While most species in
439 this genus have 21 chromosomes, *H. sapho* and *H. eleuchia eleusinus and H. e.*
440 *primularis* has 56-57 chromosomes, and *H. eleuchia eleuchia* and *H. congener* have 37

441 and 33 chromosomes, respectively (36), indicative of high rates of chromosomal fission
442 events in the group. However, even though in these species most autosomes are
443 broken up (Fig 7B-C), the chromosomes fused with the W are the full-length ancestral
444 chromosomes and thus likely did not undergo fissions. Interestingly, *H. antiochus* and *H.*
445 *hewitsoni* which also show W-A fusions have 21 chromosomes. These findings could be
446 explained by two alternative scenarios: a) The chromosomal fissions in *H. eleuchia*, *H.*
447 *congener* and *H. sapho* happened independently in each (sub)species after the W-A
448 fusions and fusing to the W protected Chr4 and Chr9/14 from fissions or b) the fissions
449 could be ancestral, and the W-fusions could have involved the largest chromosomes
450 that had not been broken up. In this second scenario, *H. hewitsoni* would have
451 undergone additional autosomal fusion events restoring chromosome number to 21 after
452 fission events. While we think the first scenario is more likely than the second one, full
453 genome assemblies will be required to distinguish these hypotheses.

454 While we cannot test for an adaptive role of the W-A fusions in the *sapho*
455 subclade, the fact that they occurred three times and remained fixed in multiple species
456 suggests they are at least not deleterious, or that any deleterious effect is masked. In
457 the latter scenario, low recombination around the W-A fusions would force their sex-
458 specific transmission and result in a permanent heterozygosity that protects against the
459 expression of deleterious recessive mutations load and favours the accumulation of
460 adaptive mutations. This is the case in inversions in *H. numata* (3,48). Other alternative
461 scenarios may have favoured the fixation of these fusions. First, a period of strong
462 genetic drift could have led to the fixation of these fusions even if they carry some

463 deleterious mutations. Second, positive natural selection acting on fusions is possible
464 (49), though it might be hard to imagine that such beneficial effects would be found on
465 all three chromosomes that fused to the W. Third, transmission bias such as meiotic
466 drive (50,51), or coincidental linkage with endosymbionts transmitted via females (e.g.
467 male-killing spiroplasma) (52) could explain how the W-A fusions might have fixed.
468 However, if chromosomal fusions occur through non-homologous recombination, meiotic
469 drive might counteract or facilitate the spread of the fusions as observed for *Leptidea*
470 butterflies (53). Fourth, the W-A fusions might have spread due to reduction of sexual
471 conflict if there are sexually antagonistic loci on Chr4/9/14. In Danaini butterflies, sex-
472 biased gene expression is consistent with this hypothesis (11). Finally, the W-A fusions
473 may have contributed to the particularly high diversification rate in this clade if they
474 linked together barrier loci in regions with reduced recombination (14).

475 This is the first genomic study focused on the *sara/sapho* clade. The inclusion of
476 multiple species and subspecies of this clade from a broad geographic range also
477 allowed us to redefine some of the relations previously reported (38), and to identify the
478 effect of geography in shaping diversity. The phylogenetic position we found for *H.*
479 *antiochus* and *H. hewitsoni* contrasts with previous amplicon based phylogenies (38,54)
480 but agrees with a recent whole genome phylogeny based on *de novo* genome
481 assemblies (55), suggesting that the phylogenetic relations we describe for these two
482 species are the most plausible. We also identified *cis* and *trans*-Andean lineages for *H.*
483 *sara* and *H. antiochus*, as well as *H. congener* and *H. eleuchia* structured by the Andes.

484 In addition, *H. sara* was the only species in which we identified Andean and Amazonian
485 lineages.

486 Further studies are needed to understand the evolutionary drivers of the W-A
487 fusions identified here, as well as their role (if any) in speciation or adaptation in this
488 clade. Our study highlights the importance of including both sexes in short-read
489 population WGS studies for identifying Sex-A fusions. Finally, we show what patterns to
490 expect if the fusions are recent enough that the previously autosomal chromosomes are
491 still diploid in both sexes. As W chromosomes are often not assembled in reference
492 genomes due to their high repeat content, genome assemblies might not necessarily
493 reveal W-A fusions. Our study thus demonstrates the power of short-read population
494 data to discover sex-A fusions, particularly for taxa where one sex is achiasmic.

495 Materials and Methods

496 Genome assembly of *Heliconius sara*

497 We used two laboratory-reared females from a stock population from Panama to
498 generate a reference genome for *H. sara* (BioSamples SAMEA8947140 and
499 SAMEA8947139; S1 Table). We assembled the genome by combining PacBio, 10X
500 data and Hi-C data, all generated by the Tree of Life Programme at the Wellcome
501 Sanger Institute (). The BioSample SAMEA8947140 was used to generate the PacBio
502 continuous long reads (CLR). Libraries were sequenced on four Single Molecule Real-

503 Time (SMRT) cells using the PacBio Sequel II system. The linked-reads from 10X
504 Genomics Chromium technology were generated with the same sample and sequenced
505 in four lanes on the Illumina HiSeq X Ten platform. The second BioSample
506 SAMEA8947139 was used to produce Dovetail Hi-C data and sequenced on a HiSeq X
507 Ten platform.

508 An initial contig assembly was generated from the PacBio (CLR) data using wtdbg2 v2.2
509 (56). The PacBio data was then used to polish the contigs using Arrow
510 (https://github.com/PacificBiosciences/GenomicConsensus). We then retained haplotig
511 identification with the Purge Haplotigs pipeline (57). The 10X data were mapped to this
512 assembly using Longranger v2.2 (10X Genomics) and variant calling was performed
513 using freebayes v1.1.0-3-g961e5f3 (58). Next, this first assembly was polished using
514 BCFtools consensus v1.9 (59) by applying homozygous non-reference calls as edits.
515 The 10X linked-reads were then used to scaffold contigs using Scaff10X v2.3
516 (https://github.com/wtsi-hpag/Scaff10X). A round of manual curation was performed on
517 these polished scaffolds using gEVAL (60). Lastly, Dovetail Genomics Hi-C data was
518 used to scaffold the assembly further using SALSA v2.2 (61), followed by another round
519 of manual curation with gEVAL (60). The chromosome-scale scaffolds were named by
520 synteny to the *Heliconius melpomene melpomene* assembly Hmel2.5 in LepBase. We
521 assessed the genome contiguity with gnx-tools (https://github.com/mh11/gnx-
522 tools/blob/master/README) and genome completeness with BUSCO v5.1.2 (62) using
523 the Lepidoptera gene set. To obtain synteny plots between *H. sara* vs. *H. melpomene*,
524 *H. erato,* and *H. charithonia*, we first performed pairwise alignments between these

genomes using minimap2 v. 2.24 (63). Subsequently, we plotted the minimap2 results using custom scripts from (https://github.com/simonhmartin/asynt).

We used whole genome resequencing data from 114 individuals obtained in this study (see sample collection for genome resequencing section) to identify the W chromosome within the genome of *Heliconius sara*. We calculated the mean depth across the scaffolds that were not yet assigned to a chromosome. We first generated a file containing the mean depth per site averaged across all individuals of the same sex and species using the --site-mean-depth option of vcftools v. 0.1.14 (64). Then, we used the R package windowscanr v. 0.1 (https://github.com/tavareshugo/WindowScanR) to calculate the average of the mean depth per species, per sex, and per 500 bp windows. Scaffolds where we observed a higher mean depth in females compared to males were assigned to the W chromosome.

Sample collection for genome resequencing

We collected 114 *Heliconius* individuals from 7 species and 18 subspecies in the *sara/sapho* clade across their distribution range: 48 *H. sara*, 2 *H. leucadia*, 21 *H. antiochus*, 13 *H. sapho*, 3 *H. hewitsoni*, 17 *H. eleuchia* and 10 *H. congener* (S1 Table). The body of each individual was preserved in NaCl-saturated DMSO solution and stored at -80°C; wings were kept for phenotype reference.

545 ## Whole-genome resequencing and genotype calling

546 Genomic DNA was extracted from thoracic tissue using a DNeasy Blood and
547 Tissue Kit (Qiagen). Library preparation and whole-genome Illumina resequencing (PE
548 reads) was carried out on Illumina's HiSeq X system by Novogene (Beijing, China), with
549 30X coverage per individual. We also downloaded two samples of *H. charithonia*
550 (SRR4032025 – SRR4032026) from SRA (https://www.ncbi.nlm.nih.gov/sra) to include
551 them as outgroups in phylogenetic analyses. Our *H. sara* genome (HelSar1) was used
552 as a reference to map the reads of each individual using BWA mem v0.7.12 (65) with
553 default parameters. We then used samtools v1.12 to sort and index the alignment files
554 (66). PCR-duplicate reads were identified and removed using Picard tools v2.9.2 (67),
555 and variant calling was conducted with Haplotype Caller (GATK, v3.7.0) in BP-resolution
556 mode (68). Then, samples were jointly genotyped using GATK's GenotypeGVCFs (68).
557 We used vcftools v0.1.14 (64) and the final VCF to calculate: (i) mean depth per
558 individual and site, (ii) quality per site, (iii) the proportion of missing data per individual
559 and (iv) the proportion of missing data per site, and (v) percentage mapping per
560 individual. Based on these results, we kept sites with quality value (--minQ) ≥ 30 and
561 less than 5% missing data. We also excluded sites with a sequencing depth below 5 and
562 mean depth per individual more than 1.5 times the mean to exclude paralogous regions.
563 For this, we used the custom script *removeTooHighDepthSites.sh* from
564 (https://github.com/joanam/VictoriaRegionSuperflock/BashPipelines). We additionally
565 removed sites with excess heterozygosity across all individuals using the vcftools option

566 --*hardy* and a p-value cut-off of <1e-5 to remove reads from paralogous regions that are
567 collapsed in the reference genome.

568 Analysis of population structure within the *sara/sapho* clade

569 We performed a principal component analysis (PCA) to study the genetic
570 structure of populations. We filtered out monomorphic or multiallelic sites, and sites with
571 minor allele frequency (MAF) smaller than 0.1 with vcftools (64). To reduce the linkage
572 disequilibrium effect, we used the python script *ldPruning.sh* from
573 (https://github.com/joanam/scripts), which removes sites with r^2>0.2 in windows of 50
574 Kbp sliding by 10 Kbp. This resulted in a vcf file with 3,685,916 high-quality SNPs sites.
575 We conducted the PCA using Plink v2.0 with default parameters (69,70).

576 Phylogenetic relationships among *sara/sapho* clade species

577 We generated a whole-genome Maximum Likelihood (ML) tree using a vcf
578 containing all sites as input in RAXML v8.2.9 (71), with the GTRGAMMA model and 100
579 bootstrap replicates. We applied the same procedure to obtain ML trees for each
580 chromosome to study the phylogenetic incongruence across the genome. We also
581 inferred the species tree using the coalescent-based method ASTRAL (72). For this, we
582 used vfctools v0.1.14 (64) to: (i) extract two males per subspecies so Sex-A fusions
583 present only in females do not alter the species tree, and (ii) extract 2 kbp loci spaced at
584 least 10 kbp apart to ensure no linkage disequilibrium between them (73). Then,

585 samtools (66) was used to generate 271 multilocus blocks, each resulting from
586 concatenating 100 loci. Each block was converted into PHYLIP format using our custom
587 script *vcf2phylip.py* from (https://github.com/joanam/scripts/blob/master/vcf2phylip.py)
588 and used to estimate a ML tree in IQ-tree (74,75) selecting the best model with
589 ModelFinder and assessing node support with 1000 ultrafast bootstraps. The resulting
590 271 topologies were used as input in ASTRAL. We also investigated these 271
591 topologies with DensiTree (76) to visualize discordance.

592 Haplotype-based phylogenetic analysis on chromosomes 4, 9 593 and 14

594 To further investigate sex clustering in the phylogenies of autosomes 4, 9 and 14,
595 we phased them to infer their haplotypes. Haplotype phasing was done by combining
596 two methods: WhatsHap, which is a haplotype assembly technique (77), and
597 SHAPEIT4, a statistical phasing method (78). To implement WhatsHap, we used the
598 BAM file of each individual as well as the reference genome to group nearby genetic
599 variants into fully resolved haplotype blocks or phase sets (77). Then, we used the
600 WhatsHap output file to run SHAPEIT4, which further phases haplotypes based on
601 population-level information using default parameters (78).

602 Next, we inferred SNP coalescent genealogies across each chromosome using
603 Relate v.1.1.2 (79). Initially, the phased vcf file was transformed into haplotype format
604 using RelateFileFormats with the “--mode ConvertFromVcf" flag. We performed this
605 analysis using an effective population size of $1x10^7$ individuals, as estimated for *H. erato*

606 (80), and a mutation rate of 2.9×10^{-9} per site per generation from *H. melpomene* (81). As
607 Relate further requires a genetic map, we created one using the average recombination
608 rate of 6 cM/Mb calculated in *H. erato* (82), and our custom script
609 (https://github.com/joanam/scripts/blob/master/createuniformrecmap.r). Finally, the
610 ancestral allele was assigned as the one more common in the outgroup *H. charithonia*.

611 Because any possible Sex-A fusion would produce heterozygous females and
612 homozygous males, we identified sites with this pattern (see hypotheses in Fig 2). We
613 first calculated the number of heterozygous and homozygous individuals per species
614 and site using the *--hardy* option in vcftools version 0.1.14 (46). Then, we used custom
615 scripts to find sites where each species in the *sapho* subclade met the following criteria:
616 (i) no males were heterozygous, (ii) at least one female was heterozygous, and (iii) not
617 more than one female was homozygous (allowing for one female with one allele not
618 called). Finally, we selected one SNP for every 1000 SNPs from these filtered sites and
619 visualized their genealogies using the script *TreeView.sh* (58). This subsampling
620 approach enabled us to examine genealogies from various sites evenly distributed along
621 the chromosomes.

622 Patterns of genetic differentiation

623 We calculated F_{ST} by pairs of sister species along chromosomes in non-
624 overlapping 50 Kbp windows. Because *H. antiochus* did not have a sister species, we
625 calculated these statistics between Andean and Amazonian subspecies. Windows that
626 contained less than 2,500 high-quality genotyped variable sites were rejected. We used

627 a dataset including SNPs and monomorphic sites and the *popgenWindows.py* script
628 from (https://github.com/simonhmartin/genomics_general). We also calculated F_{ST} per
629 sex following the same methodology.

630 Patterns of heterozygosity and mean depth by chromosome

631 To study chromosomes with F_{ST} patterns different from the genome average, we
632 used the options --het and --depth of vcftools v. 0.1.14 (62) tocalculate heterozygosity
633 and mean depth per chromosome for each individual of each species. We also
634 calculated these statistics in 50 Kbp non-overlapping sliding windows along the 'outlier'
635 chromosomes identified. On these, we calculated π specifying each individual as its own
636 population, so π became a measure of proportion of heterozygous sites. This was done
637 with the Python script *popgenWindows.py* from
638 (https://github.com/simonhmartin/genomics_general). We then averaged these values
639 across all individuals of the same sex and species. For sequencing depth, we first
640 generated a file containing the mean depth per site averaged across all individuals of
641 the same sex and species using the --site-mean-depth option of vcftools v. 0.1.14 (64).
642 We then used the R package windowscanr v. 0.1 from
643 (https://github.com/tavareshugo/WindowScanR) to calculate the mean of the mean
644 depth per species, per sex, and per window. The few individuals of *H. hewitsoni* and *H.*
645 *leucadia* were not included in the sliding windows analysis. Statistical tests were applied
646 to assess significant differences in heterozygosity and mean depth between sexes and
647 between chromosomes. As the data were not normally distributed, we performed a

648 Wilcoxon signed rank test to compare the sexes. To assess differences between
649 chromosomes, we applied a Kruskal-Wallis test and a *post hoc* test (pairwise Wilcoxon
650 test for Kruskal-Wallis).

651 Identification of fusions with Hi-C data

652 To investigate whether autosomes 4, 9, and 14 are fused with the W or Z chromosomes,
653 we constructed Hi-C libraries from the thorax of one female of *Heliconius congener*
654 (BioSamples SAMEA112329098; S1 Table) and a male of *Heliconius sapho*
655 (BioSamples SAMEA112696452, S1 Table) using the Arima2 kit (Arima Genomics, Inc).
656 These libraries were then sequenced on an Illumina NovaSeq S4 platform with 150 bp
657 paired-end reads. We used BWA mem2 v 2.2.1 (83) to map the reads against the
658 genomes of *Heliconius sara* (this study) and *Heliconius charithonia* (41) using default
659 parameters. We also mapped the Hi-C data of *H. sara* to both references to confirm the
660 absence of the fusion in the *sara* subclade. Next, we removed PCR duplicates,
661 eliminated poorly aligned reads, and filtered out reads with a mapping quality <10 from
662 the resulting BAM files using samtools v1.12 (66). Additionally, we generated contact
663 maps with pretextview and pretextSnapshot (https://github.com/wtsi-hpag/PretextView
664 and https://github.com/wtsi-hpag/PretextSnapshot). All these steps were done using a
665 custom Perl pipeline developed by Shane McCarthy at the Wellcome Sanger Institute.

666 To further investigate the excess of Hi-C contacts between autosomes 4, 14 and
667 W in the female of *H. congener*, we generated haplotype-specific Hi-C maps for these

chromosomes. First, we created a version of the *H. sara* reference genome in which chromosomes 4, 14, and W were concatenated together to allow for phasing across chromosomes. Next, we mapped the Hi-C reads of *H. congener* to this modified reference following the mapping pipeline by Arima Genomics, Inc. (). Then we called heterozygous variants using freebayes v1.3.2-dirty (58). These variants were then normalized with bcftools v1.8 (59), decomposed with vcfallelicprimitives (84) and filtered for coverage (>21 and <141 reads) with vcftools v. 0.1.14 (64). Next, the remaining SNPs were phased using HAPCUT2 v1.3.3, using both the bam and the vcf files as input (85). We used the Python script *chomper.py* from () to separate haplotype aligned HiC reads. Finally, these haplotype-specific sets of Hi-C reads were realigned to the original *H. sara* assembly using a custom Perl pipeline developed by Shane McCarthy at the Wellcome Sanger Institute. Hi-C contact map was generated using pretextview and pretextSnapshot (and https://github.com/wtsi-hpag/PretextSnapshot).

Acknowledgments

We thank “Autoridad Nacional de Licencias Ambientales—ANLA” in Colombia for granting Universidad del Rosario the collecting permit 530 and the Instituto Chico Mendes de Conservação da Biodiversidade in Brazil for granting SISBIO collection licence 59194-1 under which we performed our collecting activities. We also thank the HPC Service of Universidad del Rosario (CALDAS) for computing time. We thank the core lab of the Tree of Life Programme and the sequencing centre of the Sanger Institute for support with the HiC sequencing.

References

1. Ma WJ, Rovatsos M. Sex chromosome evolution: The remarkable diversity in the evolutionary rates and mechanisms. J Evol Biol. 2022;35(12):1581–8.

2. Abbott JK, Nordén AK, Hansson B. Sex chromosome evolution: historical insights and future perspectives. Proc R Soc B Biol Sci. 2017 May 3;284(1854):20162806.

3. Jay P, Tezenas E, Véber A, Giraud T. Sheltering of deleterious mutations explains the stepwise extension of recombination suppression on sex chromosomes and other supergenes. PLOS Biol. 2022 Jul 19;20(7):e3001698.

4. Kitano J, Ross JA, Mori S, Kume M, Jones FC, Chan YF, et al. A role for a neo-sex chromosome in stickleback speciation. Nature. 2009 Oct;461(7267):1079–83.

5. Pennell MW, Kirkpatrick M, Otto SP, Vamosi JC, Peichel CL, Valenzuela N, et al. Y Fuse? Sex Chromosome Fusions in Fishes and Reptiles. PLOS Genet. 2015 May 20;11(5):e1005237.

6. Sigeman H, Ponnikas S, Chauhan P, Dierickx E, Brooke M de L, Hansson B. Repeated sex chromosome evolution in vertebrates supported by expanded avian sex chromosomes. Proc R Soc B Biol Sci. 2019 Dec 4;286(1916):20192051.

7. Charlesworth B. Model for evolution of Y chromosomes and dosage compensation. Proc Natl Acad Sci U S A. 1978 Nov;75(11):5618–22.

8. Ross JA, Urton JR, Boland J, Shapiro MD, Peichel CL. Turnover of Sex Chromosomes in the Stickleback Fishes (Gasterosteidae). PLOS Genet. 2009 Feb 20;5(2):e1000391.

9. Zhou Q, Bachtrog D. Sex-specific adaptation drives early sex chromosome evolution in Drosophila. Science. 2012 Jul 20;337(6092):341–5.

10. Pala I, Naurin S, Stervander M, Hasselquist D, Bensch S, Hansson B. Evidence of a neo-sex chromosome in birds. Heredity. 2012 Mar;108(3):264–72.

11. Mora P, Hospodářská M, Voleníková AC, Koutecký P, Štundlová J, Dalíková M, et al. Sex-biased gene content is associated with sex chromosome turnover in Danaini butterflies. Mol Ecol. n/a(n/a):e17256.

12. Krátká M, Šmerda J, Lojdová K, Bureš P, Zedek F. Holocentric Chromosomes Probably Do Not Prevent Centromere Drive in Cyperaceae. Front Plant Sci [Internet].

2021 [cited 2023 Mar 21];12. Available from: https://www.frontiersin.org/articles/10.3389/fpls.2021.642661

13. Pardo-Manuel de Villena F, Sapienza C. Female meiosis drives karyotypic evolution in mammals. Genetics. 2001 Nov;159(3):1179–89.

14. Guerrero RF, Kirkpatrick M. Local adaptation and the evolution of chromosome fusions. Evolution. 2014 Oct;68(10):2747–56.

15. Yeaman S. Genomic rearrangements and the evolution of clusters of locally adaptive loci. Proc Natl Acad Sci U S A. 2013 May 7;110(19):E1743-1751.

16. Nguyen P, Sýkorová M, Šíchová J, Kůta V, Dalíková M, Čapková Frydrychová R, et al. Neo-sex chromosomes and adaptive potential in tortricid pests. Proc Natl Acad Sci U S A. 2013 Apr 23;110(17):6931–6.

17. Matsumoto T, Kitano J. The intricate relationship between sexually antagonistic selection and the evolution of sex chromosome fusions. J Theor Biol. 2016 Sep 7;404:97–108.

18. Schmid M, Feichtinger W, Steinlein C, Visbal García R, Fernández Badillo A. Chromosome banding in Amphibia. XXVIII. Homomorphic XY sex chromosomes and a derived Y-autosome translocation in Eleutherodactylus riveroi (Anura, Leptodactylidae). Cytogenet Genome Res. 2003;101(1):62–73.

19. Král J, Kořínková T, Krkavcová L, Musilová J, Forman M, Herrera IMÁ, et al. Evolution of karyotype, sex chromosomes, and meiosis in mygalomorph spiders (Araneae: Mygalomorphae). Biol J Linn Soc. 2013 Jun 1;109(2):377–408.

20. Maddison WP, Leduc-Robert G. Multiple Origins of Sex Chromosome Fusions Correlated with Chiasma Localization in Habronattus Jumping Spiders (araneae: Salticidae). Evolution. 2013;67(8):2258–72.

21. Flores SV, Evans AL, McAllister BF. Independent Origins of New Sex-Linked Chromosomes in the melanica and robusta Species Groups of Drosophila. BMC Evol Biol. 2008 Jan 29;8:33.

22. Charlesworth B, Coyne JA, Barton NH. The Relative Rates of Evolution of Sex Chromosomes and Autosomes. Am Nat. 1987;130(1):113–46.

23. Bressa MJ, Papeschi AG, Vítková M, Kubícková S, Fuková I, Pigozzi MI, et al. Sex chromosome evolution in cotton stainers of the genus Dysdercus (Heteroptera: Pyrrhocoridae). Cytogenet Genome Res. 2009;125(4):292–305.

24. Mongue AJ, Nguyen P, Voleníková A, Walters JR. Neo-sex Chromosomes in the Monarch Butterfly, *Danaus plexippus*. G3 GenesGenomesGenetics. 2017 Oct 1;7(10):3281–94.

25. Smith DAS, Gordon IJ, Traut W, Herren J, Collins S, Martins DJ, et al. A neo-W chromosome in a tropical butterfly links colour pattern, male-killing, and speciation. Proc R Soc B Biol Sci. 2016 Jul 27;283(1835):20160821.

26. Šíchová J, Voleníková A, Dincă V, Nguyen P, Vila R, Sahara K, et al. Dynamic karyotype evolution and unique sex determination systems in Leptidea wood white butterflies. BMC Evol Biol. 2015 Dec;15(1):89.

27. Šíchová J, Ohno M, Dincă V, Watanabe M, Sahara K, Marec F. Fissions, fusions, and translocations shaped the karyotype and multiple sex chromosome constitution of the northeast-Asian wood white butterfly, *Leptidea amurensis*. Biol J Linn Soc. 2016 Jul;118(3):457–71.

28. Carabajal Paladino LZ, Provazníková I, Berger M, Bass C, Aratchige NS, López SN, et al. Sex Chromosome Turnover in Moths of the Diverse Superfamily Gelechioidea. Barluenga M, editor. Genome Biol Evol. 2019 Apr 1;11(4):1307–19.

29. Picq S, Lumley L, Šíchová J, Laroche J, Pouliot E, Brunet BMT, et al. Insights into the Structure of the Spruce Budworm (*Choristoneura fumiferana*) Genome, as Revealed by Molecular Cytogenetic Analyses and a High-Density Linkage Map. G3 GenesGenomesGenetics. 2018 Aug 1;8(8):2539–49.

30. Yoshido A, Marec F, Sahara K. Resolution of sex chromosome constitution by genomic in situ hybridization and fluorescence in situ hybridization with (TTAGG) n telomeric probe in some species of Lepidoptera. Chromosoma. 2005 Aug;114(3):193–202.

31. Wright CJ, Stevens L, Mackintosh A, Lawniczak M, Blaxter M. Chromosome evolution in Lepidoptera [Internet]. Evolutionary Biology; 2023 May [cited 2023 Dec 28]. Available from: http://biorxiv.org/lookup/doi/10.1101/2023.05.12.540473

32. Lucek K, Augustijnen H, Escudero M. A holocentric twist to chromosomal speciation? Trends Ecol Evol. 2022 Apr;S0169534722000854.

33. White MJD. Animal Cytology and Evolution [Internet]. 3rd ed. 1977 [cited 2022 Dec 6]. Available from: https://www.cambridge.org/co/academic/subjects/life-sciences/cell-biology-and-developmental-biology/animal-cytology-and-evolution-3rd-edition, https://www.cambridge.org/co/academic/subjects/life-sciences/cell-biology-and-developmental-biology

34. Hill J, Rastas P, Hornett E, Neethiraj R, Clark N, Morehouse N, et al. Unprecedented reorganization of holocentric chromosomes provides insights into the enigma of lepidopteran chromosome evolution. Sci Adv. 2019 Jun 12;5:eaau3648.

35. Cicconardi F, Lewis JJ, Martin SH, Reed RD, Danko CG, Montgomery SH. Chromosome Fusion Affects Genetic Diversity and Evolutionary Turnover of Functional Loci but Consistently Depends on Chromosome Size. Mol Biol Evol. 2021;38(10):4449–62.

36. Brown KS, Emmel TC, Eliazar PJ, Suomalainen E. Evolutionary patterns in chromosome numbers in neotropical Lepidoptera. I. Chromosomes of the Heliconiini (family Nymphalidae: subfamily Nymphalinae). Hereditas. 1992;117(2):109–25.

37. de Castro, Zagrobelny M, Zurano JP, Zikan Cardoso M, Feyereisen R, Bak S. Sequestration and biosynthesis of cyanogenic glucosides in passion vine butterflies and consequences for the diversification of their host plants. Ecol Evol. 2019;9(9):5079–93.

38. Kozak KM, Wahlberg N, Neild AFE, Dasmahapatra KK, Mallet J, Jiggins CD. Multilocus Species Trees Show the Recent Adaptive Radiation of the Mimetic Heliconius Butterflies. Syst Biol. 2015 May 1;64(3):505–24.

39. Belleghem SMV, Rastas P, Papanicolaou A, Martin SH, Arias CF, Supple MA, et al. Complex modular architecture around a simple toolkit of wing pattern genes. Nat Ecol Evol. 2017;1(52).

40. Davey JW, Chouteau M, Barker SL, Maroja L, Baxter SW, Simpson F, et al. Major Improvements to the Heliconius melpomene Genome Assembly Used to Confirm 10 Chromosome Fusion Events in 6 Million Years of Butterfly Evolution. G3 GenesGenomesGenetics. 2016 Mar 1;6(3):695–708.

41. Chakraborty M, Lara AG, Dang A, McCulloch KJ, Rainbow D, Carter D, et al. Sex-linked gene traffic underlies the acquisition of sexually dimorphic UV color vision in Heliconius butterflies [Internet]. bioRxiv; 2022 [cited 2023 Jul 26]. p. 2022.07.04.498748. Available from: https://www.biorxiv.org/content/10.1101/2022.07.04.498748v1

42. Jiggins CD, Lamas G. The Ecology and Evolution of Heliconius Butterflies [Internet]. Oxford University Press; 2016 [cited 2022 Jul 18]. Available from: https://oxford.universitypressscholarship.com/view/10.1093/acprof:oso/9780199566570.001.0001/acprof-9780199566570

43. Rueda-M N, Salgado-Roa FC, Gantiva-Q CH, Pardo-Díaz C, Salazar C. Environmental Drivers of Diversification and Hybridization in Neotropical Butterflies.

Front Ecol Evol [Internet]. 2021 [cited 2022 Oct 31];9. Available from: https://www.frontiersin.org/articles/10.3389/fevo.2021.750703

44. QGIS Development Team. QGIS Geographic Information System. Open Source Geospatial Found Proj. 2018;URL:http://qgis.osgeo.org.

45. Suomalainen E, Cook LM, Turner JRG. Achiasmatic oogenesis in the Heliconiine butterflies. Hereditas. 1973;74(2):302–4.

46. Mackintosh A, Laetsch DR, Baril T, Foster RG, Dincă V, Vila R, et al. The genome sequence of the lesser marbled fritillary, Brenthis ino, and evidence for a segregating neo-Z chromosome. G3 GenesGenomesGenetics. 2022 Jun 1;12(6):jkac069.

47. Chen X, Wang Z, Zhang C, Hu J, Lu Y, Zhou H, et al. Unraveling the complex evolutionary history of lepidopteran chromosomes through ancestral chromosome reconstruction and novel chromosome nomenclature. BMC Biol. 2023 Nov 20;21(1):265.

48. Jay P, Chouteau M, Whibley A, Bastide H, Llaurens V, Parrinello H, et al. Mutation accumulation in chromosomal inversions maintains wing pattern polymorphism in a butterfly [Internet]. bioRxiv; 2019 [cited 2023 Oct 18]. p. 736504. Available from: https://www.biorxiv.org/content/10.1101/736504v1

49. Mackintosh A, Vila R, Martin SH, Setter D, Lohse K. Do chromosome rearrangements fix by genetic drift or natural selection? A test in Brenthis butterflies [Internet]. bioRxiv; 2023 [cited 2023 Aug 13]. p. 2023.06.16.545248. Available from: https://www.biorxiv.org/content/10.1101/2023.06.16.545248v1

50. Stewart NB, Ahmed-Braimah YH, Cerne DG, McAllister BF. Female meiotic drive preferentially segregates derived metacentric chromosomes in *Drosophila* [Internet]. Genetics; 2019 May [cited 2024 Feb 12]. Available from: http://biorxiv.org/lookup/doi/10.1101/638684

51. White MJD. Models of Speciation. Science. 1968 Mar 8;159(3819):1065–70.

52. Martin SH, Singh KS, Gordon IJ, Omufwoko KS, Collins S, Warren IA, et al. Whole-chromosome hitchhiking driven by a male-killing endosymbiont. PLOS Biol. 2020 Feb 27;18(2):e3000610.

53. Boman J, Wiklund C, Vila R, Backström N. Meiotic drive against chromosome fusions in butterfly hybrids [Internet]. bioRxiv; 2024 [cited 2024 Feb 9]. p. 2024.02.02.578558. Available from: https://www.biorxiv.org/content/10.1101/2024.02.02.578558v1

851 54. Beltrán M, Jiggins CD, Brower AVZ, Bermingham E, Mallet J. Do pollen feeding, pupal-
852 mating and larval gregariousness have a single origin in Heliconius butterflies?
853 Inferences from multilocus DNA sequence data. Biol J Linn Soc. 2007 Oct
854 1;92(2):221–39.

855 55. Cicconardi F, Milanetti E, Castro ÉCP de, Mazo-Vargas A, Belleghem SMV, Ruggieri
856 AA, et al. Evolutionary dynamics of genome size and content during the adaptive
857 radiation of Heliconiini butterflies [Internet]. bioRxiv; 2022 [cited 2022 Oct 30]. p.
858 2022.08.12.503723. Available from:
859 https://www.biorxiv.org/content/10.1101/2022.08.12.503723v1

860 56. Ruan J, Li H. Fast and accurate long-read assembly with wtdbg2. Nat Methods. 2020
861 Feb;17(2):155–8.

862 57. Roach MJ, Schmidt SA, Borneman AR. Purge Haplotigs: allelic contig reassignment
863 for third-gen diploid genome assemblies. BMC Bioinformatics. 2018 Nov 29;19(1):460.

864 58. Garrison E, Marth G. Haplotype-based variant detection from short-read sequencing
865 [Internet]. arXiv; 2012 [cited 2023 Mar 6]. Available from:
866 http://arxiv.org/abs/1207.3907

867 59. Danecek P, Bonfield JK, Liddle J, Marshall J, Ohan V, Pollard MO, et al. Twelve years
868 of SAMtools and BCFtools. GigaScience. 2021 Feb 16;10(2):giab008.

869 60. Chow W, Brugger K, Caccamo M, Sealy I, Torrance J, Howe K. gEVAL — a web-
870 based browser for evaluating genome assemblies. Bioinformatics. 2016 Aug
871 15;32(16):2508–10.

872 61. Ghurye J, Rhie A, Walenz BP, Schmitt A, Selvaraj S, Pop M, et al. Integrating Hi-C
873 links with assembly graphs for chromosome-scale assembly. PLOS Comput Biol.
874 2019 ago;15(8):e1007273.

875 62. Manni M, Berkeley MR, Seppey M, Simão FA, Zdobnov EM. BUSCO Update: Novel
876 and Streamlined Workflows along with Broader and Deeper Phylogenetic Coverage
877 for Scoring of Eukaryotic, Prokaryotic, and Viral Genomes. Mol Biol Evol. 2021 Oct
878 1;38(10):4647–54.

879 63. Li H. Minimap2: pairwise alignment for nucleotide sequences. Bioinformatics. 2018
880 Sep 15;34(18):3094–100.

881 64. Danecek P, Auton A, Abecasis G, Albers CA, Banks E, DePristo MA, et al. The variant
882 call format and VCFtools. Bioinformatics. 2011 Aug 1;27(15):2156–8.

883 65. Li H. Aligning sequence reads, clone sequences and assembly contigs with BWA-
884 MEM [Internet]. ArXiv; 2013 [cited 2022 Jul 29]. Available from:
885 http://arxiv.org/abs/1303.3997

886 66. Li H, Handsaker B, Wysoker A, Fennell T, Ruan J, Homer N, et al. The Sequence
887 Alignment/Map format and SAMtools. Bioinformatics. 2009 Aug 15;25(16):2078–9.

888 67. Broad I. Picard Toolkit [Internet]. Broad Institute; 2019 [cited 2022 Jul 29]. Available
889 from: https://github.com/broadinstitute/picard

890 68. DePristo MA, Banks E, Poplin R, Garimella KV, Maguire JR, Hartl C, et al. A framework
891 for variation discovery and genotyping using next-generation DNA sequencing data.
892 Nat Genet. 2011 May;43(5):491–8.

893 69. Chang CC, Chow CC, Tellier LC, Vattikuti S, Purcell SM, Lee JJ. Second-generation
894 PLINK: rising to the challenge of larger and richer datasets. GigaScience. 2015 Dec
895 1;4(1):s13742-015-0047–8.

896 70. Purcell S, Chang CC. PLINK: Whole genome data analysis toolset [Internet]. 2007
897 [cited 2022 Jul 29]. Available from: www.cog-genomics.org/plink/2.0/

898 71. Stamatakis A, Hoover P, Rougemont J. A Rapid Bootstrap Algorithm for the RAxML
899 Web Servers. Renner S, editor. Syst Biol. 2008 Oct 1;57(5):758–71.

900 72. Mirarab S, Reaz R, Bayzid MdS, Zimmermann T, Swenson MS, Warnow T. ASTRAL:
901 genome-scale coalescent-based species tree estimation. Bioinformatics. 2014 Sep
902 1;30(17):i541–8.

903 73. Dasmahapatra KK, Walters JR, Briscoe AD, Davey JW, Whibley A, Nadeau NJ, et al.
904 Butterfly genome reveals promiscuous exchange of mimicry adaptations among
905 species. Nature. 2012 Jul 5;487(7405):94–8.

906 74. Kalyaanamoorthy S, Minh BQ, Wong TKF, von Haeseler A, Jermiin LS. ModelFinder:
907 fast model selection for accurate phylogenetic estimates. Nat Methods. 2017
908 Jun;14(6):587–9.

909 75. Nguyen LT, Schmidt HA, von Haeseler A, Minh BQ. IQ-TREE: A Fast and Effective
910 Stochastic Algorithm for Estimating Maximum-Likelihood Phylogenies. Mol Biol Evol.
911 2015 Jan 1;32(1):268–74.

912 76. Bouckaert RR. DensiTree: making sense of sets of phylogenetic trees. Bioinformatics.
913 2010 May 15;26(10):1372–3.

77. Patterson M, Marschall T, Pisanti N, Van Iersel L, Stougie L, Klau GW, et al. WHATSHAP: Weighted Haplotype Assembly for Future-Generation Sequencing Reads. J Comput Biol. 2015 Jun;22(6):498–509.

78. Delaneau O, Zagury JF, Robinson MR, Marchini JL, Dermitzakis ET. Accurate, scalable and integrative haplotype estimation. Nat Commun. 2019 Nov 28;10(1):5436.

79. Speidel L, Forest M, Shi S, Myers SR. A method for genome-wide genealogy estimation for thousands of samples. Nat Genet. 2019 Sep;51(9):1321–9.

80. Van Belleghem SM, Baquero M, Papa R, Salazar C, McMillan WO, Counterman BA, et al. Patterns of Z chromosome divergence among Heliconius species highlight the importance of historical demography. Mol Ecol. 2018;27(19):3852–72.

81. Keightley PD, Pinharanda A, Ness RW, Simpson F, Dasmahapatra KK, Mallet J, et al. Estimation of the Spontaneous Mutation Rate in Heliconius melpomene. Mol Biol Evol. 2015 Jan 1;32(1):239–43.

82. Tobler A, Kapan D, Flanagan NS, Gonzalez C, Peterson E, Jiggins CD, et al. First-generation linkage map of the warningly colored butterfly Heliconius erato. Heredity. 2005 Apr;94(4):408–17.

83. Vasimuddin Md, Misra S, Li H, Aluru S. Efficient Architecture-Aware Acceleration of BWA-MEM for Multicore Systems. In: 2019 IEEE International Parallel and Distributed Processing Symposium (IPDPS) [Internet]. 2019 [cited 2024 Jan 20]. p. 314–24. Available from: https://ieeexplore.ieee.org/document/8820962

84. Garrison E, Kronenberg ZN, Dawson ET, Pedersen BS, Prins P. Vcflib and tools for processing the VCF variant call format [Internet]. bioRxiv; 2021 [cited 2024 Feb 12]. p. 2021.05.21.445151. Available from: https://www.biorxiv.org/content/10.1101/2021.05.21.445151v1

85. Bansal V. HapCUT2: A Method for Phasing Genomes Using Experimental Sequence Data. In: Peters BA, Drmanac R, editors. Haplotyping: Methods and Protocols [Internet]. New York, NY: Springer US; 2023 [cited 2023 Nov 3]. p. 139–47. (Methods in Molecular Biology). Available from: https://doi.org/10.1007/978-1-0716-2819-5_9

946 # Supporting information captions

947 **S1 Table. Sample information and genotyping statistics.**

948 **S2 Table. Lepidoptera genome assembly statistics.**

949 **S3 Table. BUSCO results statistics.**

950 **S1 Fig. Synteny plots showing high collinearity between *Heliconius* genomes.**

951 **S2 Fig. Identification of the W chromosome in the genome of *H. sara*.**

952 **S3 Fig. Missing data and mean depth per individual.**

953 **S4 Fig. Principal Component Analysis (PCA), performed with 3,685,916 SNPs.**

954 **S5 Fig. Species tree based on ASTRAL multi-species coalescence and Densitree**.

955 **S6 Fig. Maximum likelihood phylogeny of chromosome 1.**

956 **S7 Fig. Maximum likelihood phylogeny of chromosome 2.**

957 **S8 Fig. Maximum likelihood phylogeny of chromosome 3.**

958 **S9 Fig. Maximum likelihood phylogeny of chromosome 4.**

959 **S10 Fig. Maximum likelihood phylogeny of chromosome 5.**

960 **S11 Fig. Maximum likelihood phylogeny of chromosome 6.**

961 **S12 Fig. Maximum likelihood phylogeny of chromosome 7.**

962 **S13 Fig. Maximum likelihood phylogeny of chromosome 8.**

963 **S14 Fig. Maximum likelihood phylogeny of chromosome 9.**

964 **S15 Fig. Maximum likelihood phylogeny of chromosome 10.**

965 **S16 Fig. Maximum likelihood phylogeny of chromosome 11.**

966 **S17 Fig. Maximum likelihood phylogeny of chromosome 12.**

967 **S18 Fig. Maximum likelihood phylogeny of chromosome 13.**

968 **S19 Fig. Maximum likelihood phylogeny of chromosome 14.**

969 **S20 Fig. Maximum likelihood phylogeny of chromosome 15.**

970 **S21 Fig. Maximum likelihood phylogeny of chromosome 16.**

971 **S22 Fig. Maximum likelihood phylogeny of chromosome 17.**

972 **S23 Fig. Maximum likelihood phylogeny of chromosome 18.**

973 **S24 Fig. Maximum likelihood phylogeny of chromosome 19.**

974 **S25 Fig. Maximum likelihood phylogeny of chromosome 20.**

975 **S26 Fig. Maximum likelihood phylogeny of chromosome Z.**

976 **S27 Fig. Maximum Likelihood (ML) phylogenies inferred genome-wide and per**
977 **chromosome.**

978 **S28 Fig. Marginal tree for one SNPs in Chr4.**

979 **S29 Fig. Marginal tree for one SNPs in Chr9.**

980 **S30 Fig. Marginal tree for one SNPs in Chr14.**

981 **S31 Fig. Genome-wide divergence (F_{ST}) between pairs of species in the *sara/sapho***
982 **clade.**

983 **S32 Fig. Genome-wide divergence (F_{ST}) between pairs of subspecies of *H. eleuchia,***
984 ***H. congener* and *H. sapho*.**

985 **S33 Fig. Genome-wide divergence (F_{ST}) between pairs of subspecies of *H.***
986 ***antiochus*.**

987 **S34 Fig. Genome-wide divergence (F_{ST}) between pairs of subspecies of *H. sara*.**

988 **S35 Fig. Genome-wide divergence (F_{ST}) in the *sara/sapho* clade.**

989 **S36 Fig. Patterns of heterozygosity across the genome in the *sara/sapho* clade.**

990 **S37 Fig. Patterns of mean depth across the genome in the *sara/sapho* clade.**

991 **S38 Fig. Patterns of heterozygosity and depth across chromosome (A) 14 and (B)**
992 **9.**

993 **S39 Fig. Proportion of heterozygous sites and mean depth between sexes in sliding**
994 **windows along chromosome 4.**

995 **S40 Fig. Proportion of heterozygous sites and mean depth between sexes in sliding**
996 **windows along chromosome (A) 14 and (B) 9.**

997 **S41 Fig. The density map of Hi-C contacts confirms W-A fusions in the sapho**
998 **subclade.**